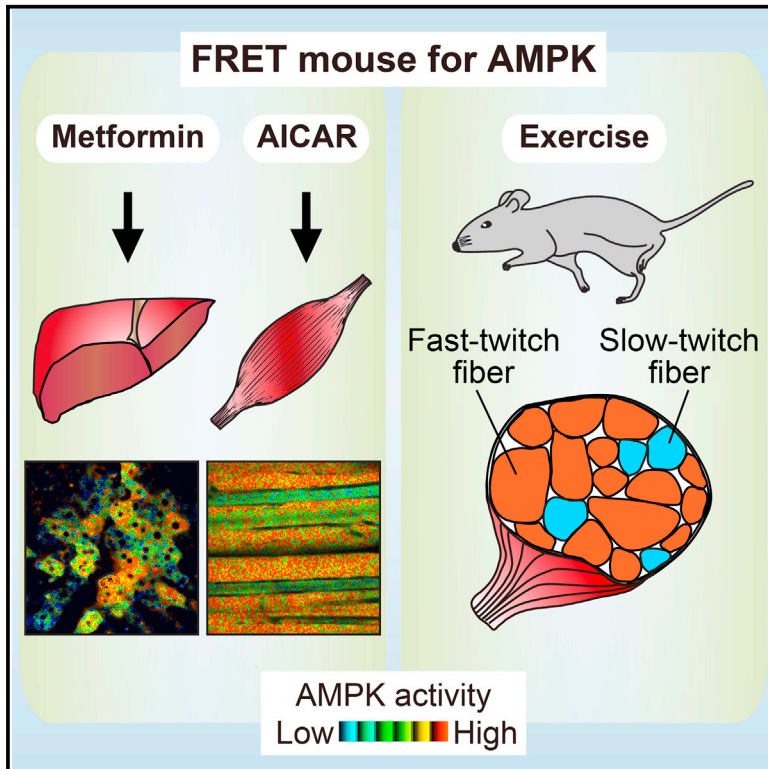


Cell Reports

A Highly Sensitive FRET Biosensor for AMPK Exhibits Heterogeneous AMPK Responses among Cells and Organs

Graphical Abstract



Authors

Yumi Konagaya, Kenta Terai, Yusuke Hirao, ..., Kenta Sumiyama, Tomoichiro Asano, Michiyuki Matsuda

Correspondence

terai.kenta.5m@kyoto-u.ac.jp

In Brief

Konagaya et al. report a highly sensitive FRET biosensor for AMP-activated protein kinase (AMPK). The biosensor readily discriminates cells with and without LKB1, a canonical AMPK activator and tumor suppressor. Transgenic mice expressing the AMPK-FRET biosensor highlight tissue-specific action of AMPK activators and fiber type-specific AMPK activation after exercise.

Highlights

- AMPK-FRET biosensor readily discriminates between cells with and cells without LKB1
- Pin1 suppresses LKB1-dependent, but not LKB1-independent, AMPK activation
- AMPK-FRET mouse visualizes cell-type-specific action of AMPK activators
- AMPK is activated mainly in fast-twitch fibers after exercise or muscle contraction



A Highly Sensitive FRET Biosensor for AMPK Exhibits Heterogeneous AMPK Responses among Cells and Organs

Yumi Konagaya,¹ Kenta Terai,^{1,8,*} Yusuke Hirao,² Kanako Takakura,³ Masamichi Imajo,¹ Yuji Kamioka,⁴ Norio Sasaoka,⁵ Akira Kakizuka,⁵ Kenta Sumiyama,⁶ Tomoichiro Asano,² and Michiyuki Matsuda^{1,7}

¹Laboratory of Bioimaging and Cell Signaling, Graduate School of Biostudies, Kyoto University, Kyoto 606-8501, Japan

²Department of Medical Science, Graduate School of Medicine, University of Hiroshima, Hiroshima 734-8553, Japan

³Imaging Platform for Spatio-Temporal Regulation, Graduate School of Medicine, Kyoto University, Kyoto 606-8501, Japan

⁴Department of Molecular Genetics, Institute of Biomedical Science, Kansai Medical University, Osaka 570-8506, Japan

⁵Laboratory of Functional Biology, Graduate School of Biostudies, Kyoto University, Kyoto 606-8501, Japan

⁶Laboratory for Mouse Genetic Engineering, Quantitative Biology Center, RIKEN, Osaka 565-0874, Japan

⁷Department of Pathology and Biology of Diseases, Graduate School of Medicine, Kyoto University, Kyoto 606-8501, Japan

⁸Lead Contact

*Correspondence: terai.kenta.5m@kyoto-u.ac.jp

<https://doi.org/10.1016/j.celrep.2017.10.113>

SUMMARY

AMP-activated protein kinase (AMPK), a master regulator of cellular metabolism, is a potential target for type 2 diabetes. Although extensive *in vitro* studies have revealed the complex regulation of AMPK, much remains unknown about the regulation *in vivo*. We therefore developed transgenic mice expressing a highly sensitive fluorescence resonance energy transfer (FRET)-based biosensor for AMPK, called AMPKAR-EV. AMPKAR-EV allowed us to readily examine the role of LKB1, a canonical stimulator of AMPK, in drug-induced activation and inactivation of AMPK *in vitro*. In transgenic mice expressing AMPKAR-EV, the AMP analog AICAR activated AMPK in muscle. In contrast, the antidiabetic drug metformin activated AMPK in liver, highlighting the organ-specific action of AMPK stimulators. Moreover, we found that AMPK was activated primarily in fast-twitch muscle fibers after tetanic contraction and exercise. These observations suggest that the AMPKAR-EV mouse will pave a way to understanding the heterogeneous responses of AMPK among cell types *in vivo*.

INTRODUCTION

The AMP-activated protein kinase (AMPK) regulates energy balance in the body (Mihaylova and Shaw, 2011; Carling et al., 2012; Hardie et al., 2012). Intracellular deficiency in ATP activates AMPK, which, in turn, promotes catabolic processes and inhibits anabolic processes by phosphorylation of multiple substrates, including acetyl-coenzyme A (CoA) carboxylase (ACC) and hydroxymethylglutaryl-CoA (HMG-CoA) reductase. The linkage of AMPK to metabolic processes renders AMPK a promising therapeutic target for obesity and type 2 diabetes (Zhang et al., 2009).

AMPK is a heterotrimeric enzyme composed of a catalytic α subunit and two regulatory β and γ subunits. The γ subunit contains four cystathionine- β synthase (CBS) domains. Each CBS domain contains a binding site for an adenosine phosphate. Sites 1 and 3 bind AMP, ADP, or ATP in a concentration-dependent manner; site 4 constitutively binds to AMP; and site 2 is always empty. Phosphorylation of Thr¹⁷² of the α subunit and allosteric activation, both due to binding of AMP to the γ subunit, lead to a 1,000-fold increase in AMPK activity (Suter et al., 2006). AMP binding to AMPK also inhibits dephosphorylation of AMPK (Davies et al., 1995). Liver kinase B1 (LKB1) is the primary protein kinase responsible for the phosphorylation of this regulatory Thr¹⁷² residue (Hawley et al., 2003; Woods et al., 2003; Shaw et al., 2004). Increased intracellular AMP concentration drives assembly of the Axin-AMPK-LKB1 complex, thereby promoting AMPK phosphorylation by LKB1 (Zhang et al., 2013). Thus, in addition to the multiple CBS domains, Axin-mediated regulation contributes to the ultrasensitive system for the monitoring of intracellular AMP concentration.

Calcium/calmodulin-dependent protein kinase kinase 2 (CaMKK2, also known as CaMKK β) has also been shown to phosphorylate Thr¹⁷² of the α subunit in a calcium-dependent manner (Hurley et al., 2005; Hawley et al., 2005). This pathway is known to function at least in neurons and T cells (Mihaylova and Shaw, 2011; Carling et al., 2012; Hardie et al., 2012).

Another class of AMPK regulator is peptidyl-prolyl *cis/trans* isomerase (PPIase) NIMA-interacting 1 (Pin1), which binds to a number of proteins and regulates oncogenesis and metabolic diseases (Khanal et al., 2013; Zhou and Lu, 2016). Pin1 has been shown to bind to and inhibit AMPK; therefore, at least some effects of Pin1 on metabolism appear to be mediated by the Pin1-AMPK association.

The AMPK activity has been studied extensively by *in vitro* kinase assay and immunoblotting with anti-phospho-AMPK (pAMPK) or anti-phospho-ACC (pACC), which reflect mean AMPK activity in the cell population. To examine the heterogeneity of AMPK activity, Tsou et al. (2011) developed AMPKAR, a genetically encoded biosensor based on fluorescence

resonance energy transfer (FRET) for AMPK activity, and revealed a very high cell-to-cell heterogeneity in the amplitude and time course using tissue culture cells. An improved version of AMPKAR has been developed and used to examine the AMPK activity in neurons (Sample et al., 2015). A drawback of many FRET biosensors, including AMPKAR, may be low signal-to-noise ratio. We have reported that a long, flexible EV linker could significantly improve the dynamic range of many FRET biosensors by reducing the basal FRET signal (Komatsu et al., 2011) and that the resulting highly sensitive FRET biosensors enable us to visualize protein kinase activities in living mice, collectively called FRET mice (Kamioka et al., 2012).

In this study, we have applied the EV linker technology to AMPKAR. The resulting AMPKAR-EV FRET biosensor exhibits three-fold higher dynamic range than AMPKAR and monitored AMPK activation in HeLa cells stimulated by 2-deoxyglucose (2-DG). Moreover, intravital imaging of transgenic mice expressing AMPKAR-EV has revealed that AMPK is predominantly activated in fast-twitch muscle fibers and that metformin activates AMPK in hepatocytes, but not in muscles. Thus, the *in vivo* imaging of AMPK activity will open a window to understanding the heterogeneous responses of AMPK among cell types *in vivo*.

RESULTS

AMPKAR-EV Monitors the Effect of Stimulators and an Inhibitor on Endogenous AMPK Activity

AMPKAR is a genetically encoded intramolecular FRET biosensor for monitoring AMPK activity in living cells (Tsou et al., 2011). We developed AMPKAR-EV to increase the sensitivity by using a long, flexible EV linker (Komatsu et al., 2011), and by replacing the yellow fluorescent protein (YFP) with YFP for energy transfer (YPet), a FRET-prone variant of YFP (Nguyen and Daugherty, 2005). Phosphorylation of the substrate peptide by AMPK promotes its binding to the FHA1 domain and a conformational change of AMPKAR-EV, resulting in an increase in the FRET efficiency from super enhanced cyan fluorescent protein (SECFP) to YPet (Figure 1A). The fluorescence ratio of YPet to SECFP, hereinafter the FRET/CFP ratio, is used to represent the FRET efficiency. HeLa cells transiently expressing AMPKAR-EV were stimulated with 10 mM 2-DG, a glucose analog that perturbs glycolysis and reduces cytosolic ATP levels. We performed a side-by-side experiment with the prototype AMPKAR (Figures 1B and 1C). In contrast to the prototype AMPKAR, AMPKAR-EV exhibited a remarkably low FRET/CFP ratio, primarily because the EV linker decreases the association of SECFP and YPet in the absence of phosphorylation of the substrate (Komatsu et al., 2011). After 2-DG stimulation, AMPKAR-EV, but not the prototype AMPKAR, showed a robust and rapid change in the FRET/CFP ratio. The low response of the prototype AMPKAR to 2-DG in HeLa cells agrees with the previous report (Tsou et al., 2011). To examine the correlation of the FRET/CFP ratio with AMPK activity, immunoblotting experiments and FRET imaging were performed side by side in HeLa cells stably expressing AMPKAR-EV. The temporal dynamics of pACC levels were similar to those of AMPKAR-EV (Figure 1C). Moreover, 2-DG-induced phosphorylation of ACC was correlated almost linearly with the FRET/CFP ratio (correlation coefficient

= 0.92 and 0.95) (Figure 1D). We also tested whether the increase in the FRET/CFP ratio required endogenous AMPK by using AMPK-double knockout (DKO) HEK293A cells, which lack both AMPK α 1 and AMPK α 2 (PRKAA1 and PRKAA2) genes. The basal FRET/CFP ratio was markedly higher in the wild-type (WT) HEK293A cells than in the AMPK-DKO HEK293A cells (Figure 1E). Moreover, 2-DG increased the FRET/CFP ratio only in WT HEK293A cells. Thus, AMPKAR-EV is specific to AMPK and sensitive enough to detect 2-DG-stimulated AMPK activation.

We further examined the response of AMPKAR-EV for two AMPK stimulators that have different modes of action. A-769662 is a thienopyridone and directly activates AMPK by inducing interaction between the β and the γ subunits of AMPK (Göransson et al., 2007; Xiao et al., 2013). On the other hand, 5-aminoimidazole-4-carboxamide-1- β -D-ribofuranoside (AICAR) is phosphorylated to yield an AMP analog, 5-aminoimidazole-4-carboxamide-1- β -D-ribofuranotide (ZMP), which binds to AMPK and thereby promotes net phosphorylation by LKB1 (Corton et al., 1995; Zhang et al., 2013). A-769662 induced a rapid increase in the FRET/CFP ratio in AMPKAR-EV-expressing Colon 38 cells (Figure 1F). The temporal dynamics of the FRET/CFP ratio were comparable to those of pACC. Dose responses revealed that the 50% effective concentration (EC₅₀) of A-769662 was \sim 50 μ M under our experimental conditions (Figure 1G). Similarly, the EC₅₀ of AICAR was determined as \sim 0.5 mM in Colon 38 cells. These values are similar to those reported previously (Cool et al., 2006; Göransson et al., 2007). Altogether, these results support the notion that AMPKAR-EV faithfully represents AMPK activity in tissue culture cells.

AMPKAR-EV Delineates Roles of LKB1 in the Basal Activity and Drug-Induced Activation of AMPK Activity

LKB1, a major regulator of AMPK (Hawley et al., 2003; Woods et al., 2003; Shaw et al., 2004), is often suppressed in cancer cells. We therefore examined whether the basal AMPK activity detected by AMPKAR-EV correlated with the expression of LKB1. We used HepG2, Colon 38, and 3LL cells as cell lines retaining intact LKB1 and used A549, H460, and HeLa cells as cell lines deficient for LKB1. As expected, ACC was more phosphorylated in LKB1-intact cells than that in LKB1-deficient cells, although the level of phosphorylation differed significantly among the LKB1-intact cells (Figure S1). In agreement with this observation, the FRET/CFP ratio clearly grouped the cell lines into LKB1-positive and LKB1-negative cell lines (Figure 2A). Consistently, HeLa cells exhibited high basal AMPK activity by the expression of WT, but not by that of kinase-deficient LKB1.

We further examined the cellular response to AICAR, metformin, 2-DG, and A-769662, which have been shown to activate AMPK in an LKB1-dependent or LKB1-independent manner. Metformin is one of the most widely used anti-diabetic drugs; it acts by inhibiting respiratory-chain complex I and thereby increasing the AMP/ATP ratio (Viollet et al., 2012). As reported previously (Shaw et al., 2004; Shackelford et al., 2013), AICAR and metformin increased the FRET/CFP ratio in the LKB1-expressing cell lines Colon 38, HepG2, and 3LL, but not in the LKB1-deficient cell lines A549, H460, and HeLa (Figure 2B). In contrast to AICAR and metformin, 2-DG induced a rapid and

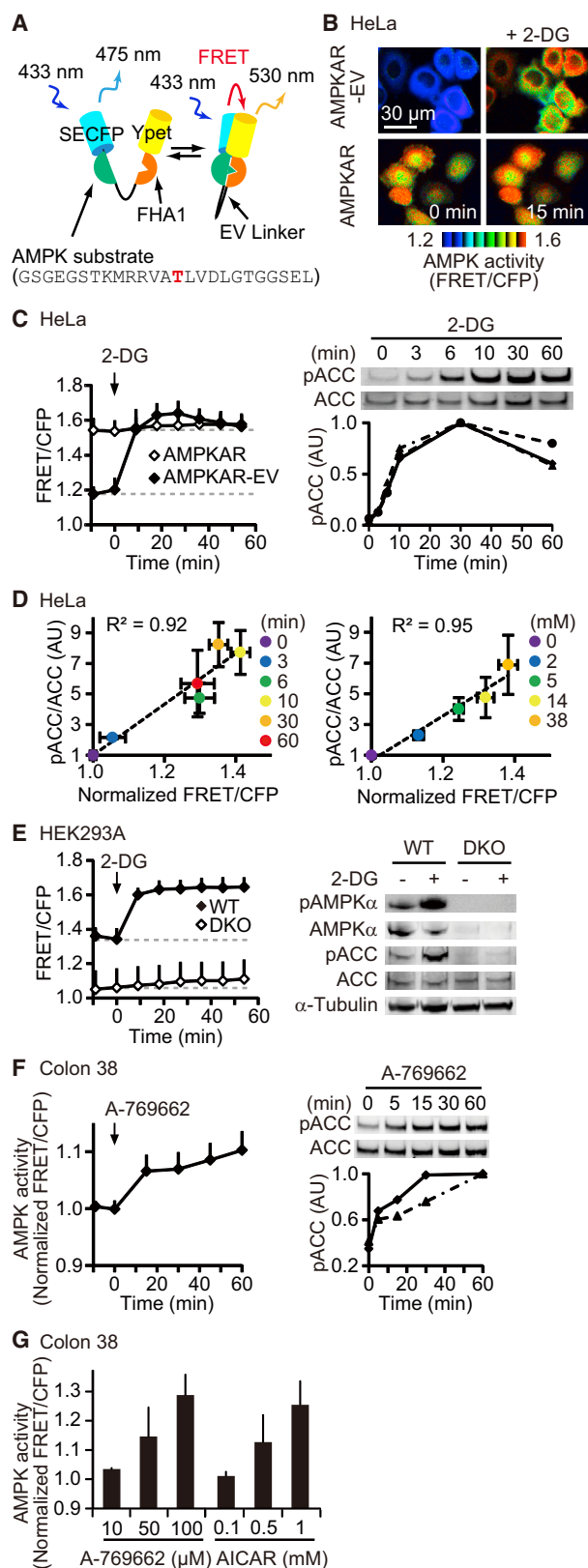


Figure 1. AMPKAR-EV Monitors the Effect of Stimulators and an Inhibitor on Endogenous AMPK Activity

(A) A schema of AMPKAR-EV is shown. (B and C) Representative FRET/CFP ratio images at the indicated time points are shown in the intensity-modulated display (IMD) mode (B). HeLa cells expressing AMPKAR-EV were stimulated with 10 mM 2-deoxyglucose (2-DG) at 0 min. The averaged FRET/CFP ratios are also shown (bars, SDs; $n = 20$ cells across 4 or 5 fields of view). Gray dashed lines denote the initial values. The time course of pACC (Ser⁷⁹) and total ACC following addition of 10 mM 2-DG in HeLa cells was analyzed by immunoblotting (top) and quantified (bottom). The level of pACC was normalized by the maximum value ($n = 3$ independent samples) (C). (D) Phosphorylation of ACC (pACC/ACC) is plotted against FRET/CFP. HeLa cells expressing AMPKAR-EV were stimulated with 10 mM 2-DG at the indicated time points (left) or stimulated with the indicated concentrations of 2-DG at 20 min (right). The levels of pACC and the averaged FRET/CFP ratios were normalized by 0 min (left) or 0 mM (right). The dashed lines denote the linear regression line with a coefficient of determination $R^2 = 0.92$ (left) and $R^2 = 0.95$ (right) (bars, SDs; $n = 3$ independent experiments). (E) Similar experiments were performed as in (C) using the WT and AMPK-double knockout (DKO) HEK293A cells. Cells were analyzed before and 20 min after 2-DG treatment for immunoblotting. (F) Similar experiments were performed as in (C) using Colon 38 cells expressing AMPKAR-EV with 50 μ M A-769662 (bars, SDs; $n =$ more than 8 cells across 3 fields of view). (G) Colon 38 cells expressing AMPKAR-EV were stimulated with A-769662 or AICAR at the indicated concentrations. The averaged FRET/CFP ratios at 60 min after the stimulation were normalized by the values before the stimulation (bars, SDs; $n =$ more than 4 cells across 4 or 2 fields of view).

sustained increase in the FRET/CFP ratio irrespective of the expression of LKB1. We found that A-769662 elicited two phases of AMPK activation: a rapid and transient increase 10 to 20 min after the stimulation and a gradual second-phase increase after 30 min. The mechanism of this two-phase increase is unknown.

Because the increase in the FRET/CFP ratio by 2-DG was also observed in LKB1-deficient cells, we examined the contribution of the Ca²⁺-CaMKK2 pathway to 2-DG-induced AMPK activation. As expected, the intracellular Ca²⁺ chelator BAPTA-AM, the CaMKK2 inhibitor STO-609, and a small interfering RNA (siRNA) against CaMKK2 ablated the 2-DG-induced increase in the FRET/CFP ratio (Figure S2A). The consistent effect of the CaMKK2 was confirmed by immunoblotting with anti-pACC antibody (Figure S2B). Similar results were obtained using A549 (Figures S2C and S2D). By using R-GECO1.0, which is a Ca²⁺ indicator, we confirmed that intracellular Ca²⁺ levels were increased upon 2-DG stimulation, irrespective of AMPKAR-EV expression (Figure S2E). All of these results are consistent with the idea that the 2-DG-induced AMPK activation in LKB1-deficient cell lines depends on the Ca²⁺-CaMKK2 pathway and that AMPKAR-EV faithfully reports the AMPK activity in the presence of various stimulators and inhibitors.

Pin1 Inhibits LKB1-Dependent, but not CaMKK2-Dependent, AMPK Activation

Pin1, a PPIase, has been shown to suppress AMPK by direct binding to phospho-Ser¹⁷⁶ of AMPK (Khanal et al., 2013) and phospho-Thr²¹¹ of AMPK (Nakatsu et al., 2015). However, it has not been determined whether Pin1 inhibits both LKB1- and CaMKK2-dependent AMPK activation. To answer this question, we examined the effect of Pin1 on AMPK activity in the presence

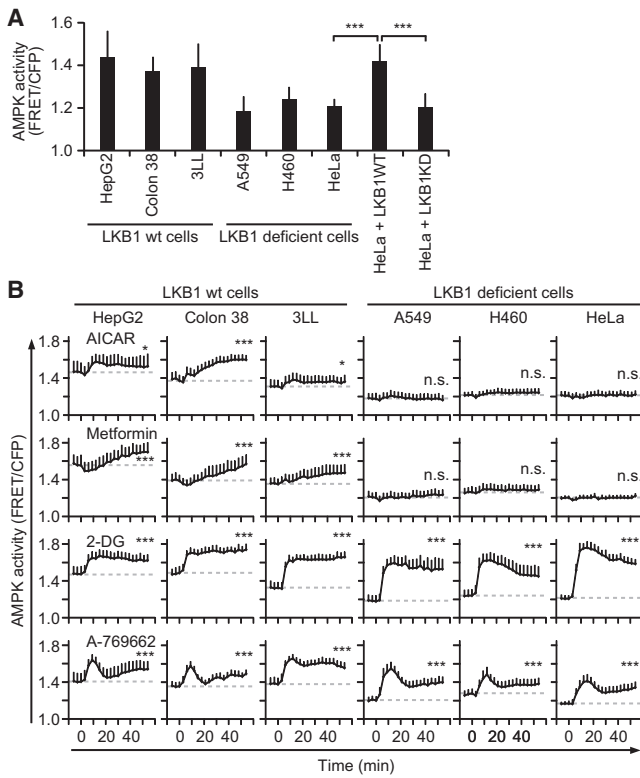


Figure 2. AMPKAR-EV Delineates Roles of LKB1 in the Basal and Drug-Induced AMPK Activity

(A) The averaged FRET/CFP ratios of AMPKAR-EV in different cell lines without stimulation are shown (bars, SDs; $n = 2$ independent experiments with 15 cells; $***p < 0.001$). HepG2, Colon 38, and 3LL cells express LKB1, while A549, H460, and HeLa cells are LKB1 deficient, as shown in Figure S1. LKB1 or kinase-dead LKB1 was expressed in HeLa cells (HeLa + LKB1WT and HeLa + LKB1KD, respectively).

(B) Cells expressing AMPKAR-EV were stimulated with the following agents: 10 mM 2-DG, 50 μ M A-769662, 1 mM AICAR, and 10 mM metformin. The averaged FRET/CFP ratios are shown (bars, SDs; $n =$ more than 16 cells across more than 3 fields of view). Gray dashed lines denote the initial values. Statistical significance of the averaged FRET/CFP was assessed between the initial time point and 54 min after the stimulation ($***p < 0.001$; $*p < 0.05$; n.s., not significant). See also Figures S1 and S2.

or absence of LKB1. We found that the basal FRET/CFP ratios were decreased by Pin1 overexpression in LKB1-expressing cells, including HepG2 cells, Colon 38 cells, and LKB1-expressing HeLa cells, but not in the authentic LKB1-deficient HeLa cells (Figure 3A). By contrast, Pin1 inhibitors increased the FRET/CFP ratio only in the LKB1-expressing HeLa cells, not in the authentic HeLa cells (Figure 3B). Collectively, these results indicate that Pin1 inhibits LKB1-dependent AMPK activation under unstimulated conditions. Next, therefore, we examined the effect of Pin1 under stimulated conditions. The authentic and LKB1-expressing HeLa cells were infected with Pin1-expressing lentivirus and time-lapse imaged to examine the effect of AMPK stimulators (Figures 3C and 3D). In the authentic HeLa cells, AICAR failed to exhibit any effects irrespective of the expression of Pin1. In the LKB1-expressing HeLa cells, Pin1 not only decreased the basal FRET/CFP ratio but also abrogated AICAR-induced increase in

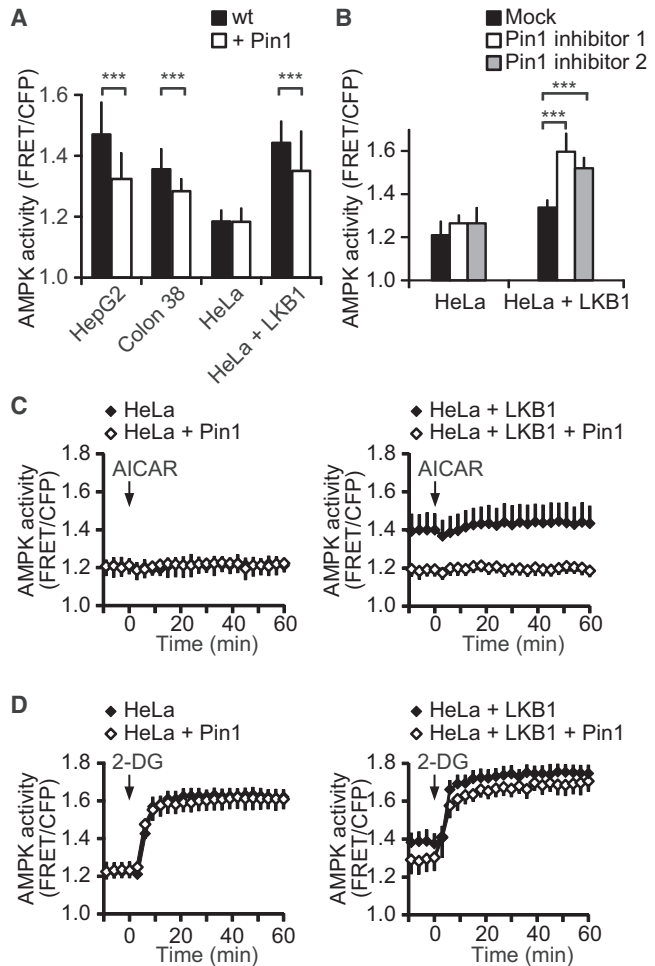


Figure 3. Pin1 Inhibits LKB1-Dependent AMPK Activation

(A) Pin1 was overexpressed in HepG2, Colon 38, HeLa, and HeLa + LKB1 cells. The averaged FRET/CFP ratios of AMPKAR-EV in different cell lines are shown (bars, SDs; $n = 3$ independent experiments with 19 to 20 cells each; $***p < 0.001$).

(B) HeLa and HeLa + LKB1 cells were stimulated with 100 μ M of Pin1 inhibitor 1 or 2 for 30 min. The averaged FRET/CFP ratios are shown (bars, SDs; $n = 3$ independent experiments with 3 to 11 cells each; $***p < 0.001$).

(C and D) HeLa and HeLa + LKB1 cells with or without overexpression of Pin1 were stimulated with 1 mM AICAR (C) and 10 mM 2-DG (D). The averaged FRET/CFP ratios of the cells are shown (bars, SDs; $n =$ more than 20 cells across more than 3 fields of view).

See also Figure S2.

the FRET/CFP ratio. In contrast to AICAR, 2-DG markedly increased the FRET/CFP ratio, irrespective of the presence of LKB1 or Pin1 (Figure 3D). Because we have shown that 2-DG activates AMPK via the Ca^{2+} -CaMKK2 pathway (Figure S2), these results demonstrated that Pin1 inhibits LKB1-dependent, but not CaMKK2-dependent, AMPK activation.

Myocytes and Hepatocytes Respond to AICAR and Metformin Differently

Encouraged by the *in vitro* data showing that AMPKAR-EV could monitor AMPK activity under various conditions, we generated

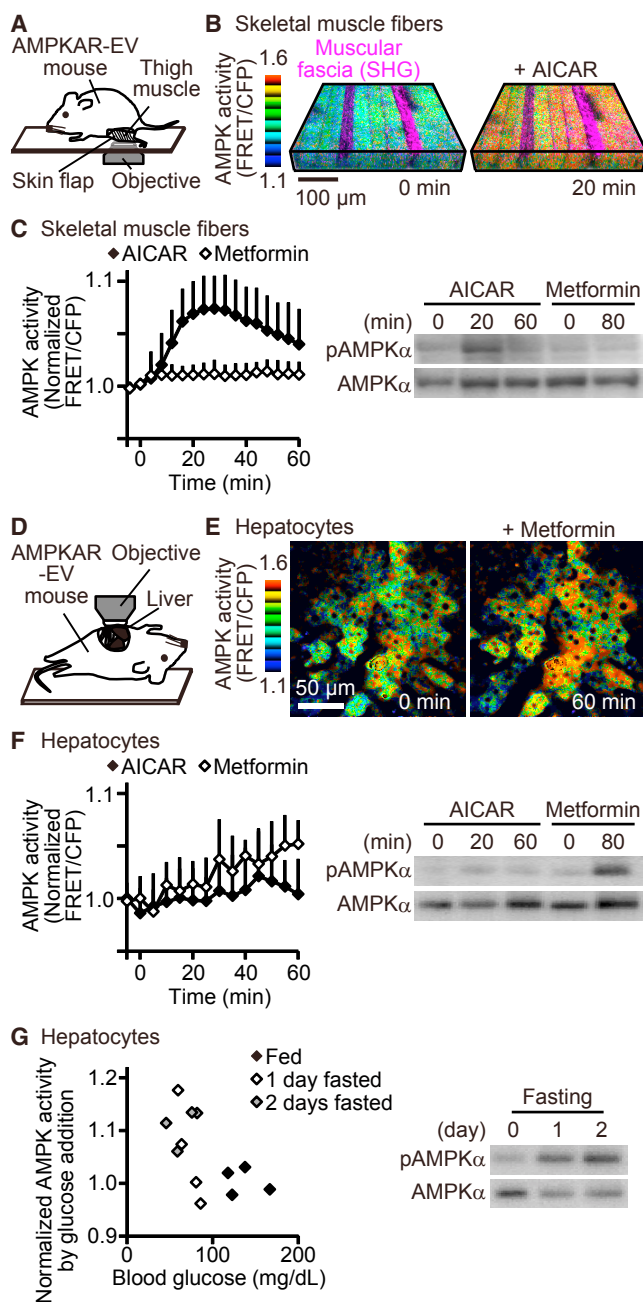


Figure 4. Myocytes and Hepatocytes Respond to AICAR and Metformin Differently

(A–F) Layout of the intravital imaging system for the biceps femoris (A) and the liver (D). An anesthetized mouse is placed on an electric heat pad and observed with an inverted or an upright two-photon excitation microscope. Representative FRET/CFP ratio images of the biceps femoris (B) and the liver (E) at the indicated time points are shown in IMD mode. AICAR (250 mg/kg) or metformin (100 mg/kg) was injected intravenously at 0 min. (C and F) The averaged FRET/CFP ratios are shown (bars, SDs; $n = 3$ independent experiments with more than 32 skeletal muscle fibers [C] and 6 hepatocytes [F]). pAMPK (Thr¹⁷²) and total AMPK following addition of AICAR or metformin were also analyzed by immunoblotting.

(G) Normalized FRET/CFP is plotted against blood glucose levels. AMPKAR-EV mice were fasted for more than 24 or 48 hr. AMPKAR-EV mice fed *ad libitum*

transgenic mice expressing AMPKAR-EV by Tol2-mediated gene transfer (Kamioka et al., 2012). The transgenes were transmitted to offspring by Mendelian inheritance across five generations (continued transmission in this line is ongoing). Animals transgenic for FRET biosensors grew normally and showed no external or internal signs of malformations or other adverse reactions to the transgene. The CAG promoter-driven expression of AMPKAR-EV was sufficiently robust to identify newborn transgenic mice by visual inspection of green fluorescence in the skin. Expression of AMPKAR-EV was confirmed in most, if not all, organs examined by visual inspection and *in vivo* imaging by two-photon excitation microscopy.

One of the prospective applications of FRET mice is for the study of pharmacodynamics. Here, we attempted to visualize the effect of AICAR and metformin in the liver and the skeletal muscle (Figure 4). In muscle cells, AICAR, but not metformin, induced a transient increase in the FRET/CFP ratio (Figures 4B and 4C; Movie S1). In contrast, the FRET/CFP ratio in hepatocytes was gradually increased only by metformin (Figures 4E and 4F). Immunoblotting analysis confirmed the organ-specific effect of AICAR and metformin on pAMPK levels. Thus, these data demonstrate that the AMPKAR-EV mouse is a powerful tool for comparing the pharmacodynamics of stimulators and inhibitors of AMPK among different tissues. We also examined whether we could detect AMPK activation upon starvation. For this, mice were starved for one or two days, and AMPK activity was monitored in the liver (Figure 4G). Hepatocytes in starved mice showed higher FRET efficiency than those in fed mice, representing that the AMPKAR-EV mouse reports the AMPK activation under a physiological stimulus. We also confirmed the effect of starvation in each mouse by measuring blood glucose levels and AMPK phosphorylation (Figure 4G).

AMPKAR-EV Mice Reveal AMPK Activation in Fast-Twitch Fibers after Contraction *In Vivo*

Another promising application of the transgenic mice expressing AMPKAR-EV is for the examination of heterogeneous responses of cell types within a tissue of interest. In skeletal muscles, fibers are largely classified into white fast-twitch muscles, characterized by glycolytic metabolism, and red slow-twitch muscles, characterized by oxidative metabolism. We examined whether any muscle fiber type-specific difference could be observed in the AMPK activity by observing the biceps femoris after tetanic contraction or exercise. After stimulation, mice were subjected to *in vivo* imaging. To increase the number of muscle fibers to be analyzed, one to four fields of view were imaged in each mouse. The image acquisition started approximately 5 min and no later than 31 min after the stimulation; in no case were images captured later than 40 min after the stimulation. Precise intervals between the stimulation and the imaging are described in Figure S3.

were used as a control. Glucose (1 g/kg) was injected intravenously at 0 min. The averaged FRET/CFP ratios just before the glucose addition were normalized by the values 60 min after the stimulation ($n = 4$ independent experiments with more than 15 hepatocytes). pAMPK (Thr¹⁷²) and total AMPK after starvation were also analyzed by immunoblotting. Refer to Movie S1.

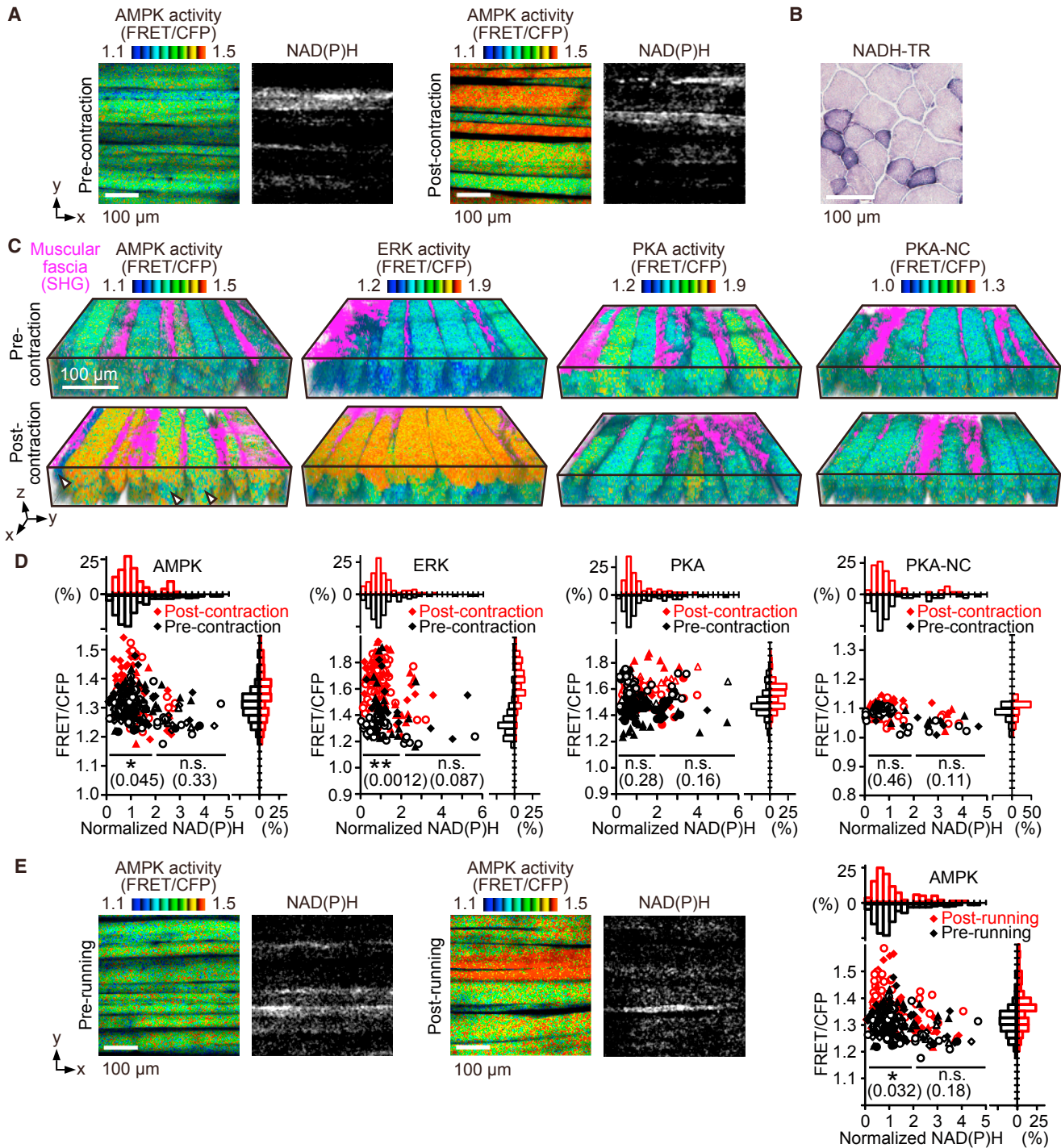


Figure 5. AMPKAR-EV Mice Reveal AMPK Activation in Fast-Twitch Fibers after Contraction In Vivo

(A) Representative FRET/CFP ratio images of the skeletal muscle fibers are shown in IMD mode. NAD(P)H images were obtained at 430 nm fluorescence. Muscle contraction was electrically induced in the AMPKAR-EV mice.

(B) Muscle fiber types were assessed by NADH tetrazolium reductase (NADH-TR) staining.

(C) Representative FRET/CFP ratio images of the skeletal muscle fibers are shown in IMD mode. Transgenic mice expressing FRET biosensors for AMPK, ERK, PKA, and a negative control underwent electrical induction of muscle contraction. Image acquisition was started 5 to 31 min after the end of stimulation and finished in 40 min. See also Figure S3 for the detailed interval between the stimulation and the *in vivo* imaging. White arrowheads indicate NAD(P)H-high fibers.

(D) The FRET/CFP ratio is plotted against normalized NAD(P)H intensity. To minimize the depth effect, NAD(P)H intensity was normalized by dividing the average of the entire image. 10 to 50 fibers in each mouse were imaged, quantified, and presented in the figure. Each shape (triangles, circles, or diamonds) represents the

(legend continued on next page)

In the control mice, the FRET/CFP ratio in each muscle fiber differed to some extent; however, the heterogeneity was significantly increased after electrically induced tetanic contraction (Figure 5A). Fluorescence of 430 nm can be used to quantify NAD(P)H and thereby identify the muscle fiber types, because NAD(P)H is abundant in mitochondria-rich, red slow-twitch muscle fibers (Piston et al., 1995; Rothstein et al., 2005). We found that NAD(P)H-high fibers were smaller in diameter and lower in FRET/CFP ratio than NAD(P)H-low fibers (Figure 5A). The proportion and diameter of NAD(P)H-high fibers were similar to those of fibers heavily stained by NADH-TR, supporting the muscle fiber typing by NAD(P)H fluorescence (Figure 5B). We extended this approach to examine the specificity of our findings by using transgenic mice expressing FRET biosensors for ERK and PKA and a negative control FRET biosensor, PKA-NC (Figure 5C). Quantification of the FRET/CFP ratio and NAD(P)H intensity demonstrated clearly that AMPK was activated preferentially in NAD(P)H-low fibers 0 to 40 min after electronically induced tetanic contraction (Figure 5D). Similar results were obtained for ERK. Upon muscle contraction, the FRET/CFP ratio in transgenic mice expressing the FRET biosensor for ERK was significantly increased in NAD(P)H-high muscle fibers. The increase in the FRET/CFP ratio was mostly confined to the muscle fibers beneath the muscular fascia, suggesting that the ERK activity was regulated not by the type of muscle fibers but rather by the location within the muscle. In contrast, the transgenic mice expressing the FRET biosensor for PKA or the negative control FRET biosensor did not show a significant increase in the FRET/CFP ratio in the muscle. Collectively, these data suggest that AMPK is activated in fast-twitch fibers after tetanic contraction.

Finally, we investigated whether treadmill exercise is able to activate AMPK in fast-twitch fibers specifically. Mice were trained according to a previous report (Maarbjerg et al., 2009) and then forced to run on a treadmill for 60 min at 16 m/min. After treadmill running, there were some myofibers with high AMPK activity, especially in NAD(P)H-low fibers (Figure 5E). This result supports our model that AMPK is activated in fast-twitch fibers. In conclusion, the transgenic mouse expressing AMPKAR-EV is a powerful tool to detect the minor population and examine the heterogeneous responses of AMPK *in vivo*.

DISCUSSION

By the use of a flexible EV linker, the basal level of the FRET/CFP ratio was markedly decreased in comparison to that for the prototype, AMPKAR (Figures 1B and 1C). This decreased basal signal of AMPKAR-EV allowed us to classify cells easily into two groups based on the expression of LKB1 (Figure 2). In agreement with previous reports (Hawley et al., 2003; Woods et al., 2003;

Shaw et al., 2004; Gowans et al., 2013), this significant difference in the basal AMPK activity indicates that LKB1 phosphorylates and activates AMPK even in nutrient-rich culture medium. It should be recalled that AMPK-dependent phosphorylation inactivates ACC and HMG-CoA reductase. Thus, the basal activities of LKB1 and AMPK may play a role in reserving inert ACC and HMG-CoA reductase. In this context, we may need to pay more attention to signals that reduce LKB1 activity under nutrient-rich conditions.

Pin1 has been shown to bind to and inactivate AMPK (Khanal et al., 2013; Nakatsu et al., 2015). The binding of Pin1 to the CBS3 domain of the AMPK γ subunit exposes phospho-Thr¹⁷² of the α subunit for the dephosphorylation by PP2C and thereby suppresses AMPK activity (Nakatsu et al., 2015). By using cell lines expressing AMPKAR-EV, we found that Pin1 inhibits AMPK activation by LKB1, but not by CaMKK2 (Figures 3 and S2), suggesting an LKB1-specific mechanism of inhibition. LKB1 phosphorylates AMPK on a scaffold protein, Axin (Zhang et al., 2013). It remains unknown which subunit of AMPK binds to Axin; however, we could speculate that Pin1 binding to AMPK inhibits the association of AMPK with Axin and thereby prevents AMPK from LKB1-dependent phosphorylation. This scenario can also explain why Pin1 did not inhibit CaMKK2-dependent AMPK activation.

The difference in the AMPK activity between slow- and fast-twitch fibers has been controversial. Narkar et al. (2011) found that AMPK was more active in the soleus (predominantly slow-twitch myofibers) than the quadriceps (predominantly fast-twitch myofibers). Meanwhile, other research groups failed to find significant difference in AMPK activity between the soleus and the extensor digitorum longus (predominantly fast-twitch myofibers) (Dzamko et al., 2008; Jensen et al., 2007; Jørgensen et al., 2004). These studies were based mostly on immunoblotting with anti-pAMPK; therefore, they do not necessarily show the difference between fast- and slow-twitch fibers. The use of AMPKAR-EV enabled us to examine the AMPK activity directly in each fiber type before and after stimulation (Figure 5). Our data strongly suggested that only the fast-twitch myofibers exhibited an increase in AMPK activity upon tetanic contraction and exercise. We may speculate that the tetanic contraction and the exercise causes ATP consumption primarily in fast-twitch myofibers, resulting in strong AMPK activation. Although we cannot rule out the possibility that AMPK activation in the slow-twitch myofibers was transient, and therefore could not be detected in our experimental protocol, it is unlikely that such transient AMPK activation alters the metabolic states of the slow-twitch myofibers. It would be interesting to test whether low-intensity, long-time exercise may activate AMPK preferentially in the slow-twitch myofibers.

dataset from the same mouse before and after stimulation. Histograms of the normalized NAD(P)H intensity and FRET/CFP ratio are shown at the top and right side of the figure, respectively. For statistical analysis, the datasets were divided into two groups by the threshold of normalized NAD(P)H = 2. Statistical significance of the averaged FRET/CFP was assessed by t test between before and after stimulation in categorized fibers (** $p < 0.01$; * $p < 0.05$; n.s., not significant; p values are given in parentheses).

(E) Similar experiments were performed as in (D). Trained mice expressing AMPKAR-EV were run on a treadmill for 60 min at 16 m/min. Image acquisition was started 6 to 25 min after the end of running and finished in 40 min. AMPKAR-EV mice without training were used as a control (* $p < 0.05$; n.s., not significant; p values are given in parentheses).

Because of the critical roles played by AMPK in energy sensing and cancer cell survival, a huge number of drugs have been proposed to exert their pharmacological effects by means of AMPK activation (Kim and He, 2013). For example, metformin has been shown to activate AMPK in muscle (Sajan et al., 2010; Kristensen et al., 2014), liver (Shaw et al., 2005; Sajan et al., 2010; Tajima et al., 2013), brain (Chen et al., 2009; Duan et al., 2013; Cho et al., 2015), and pancreatic cancer cells (Hinke et al., 2007; Kisfalvi et al., 2009; Sinnett-Smith et al., 2013); however, the difficulty of performing direct comparisons among experimental setups renders the effect of metformin obscure, even if we admit the pleiotropic effects of this agent. Intravital imaging of AMPK activity by using AMPKAR-EV-expressing transgenic mice has enabled us to visualize the influence of AMPK-activating reagents to different organs on the same scale. We found that effect of metformin on AMPK activity differs substantially between liver and skeletal muscle (Figure 4). The reason for this tissue-specific action of metformin is probably because a metformin transporter, organic cation transporter 1 (OCT1), is expressed preferentially in the liver (Wang et al., 2002). Similarly, the expression level of OCT1 in each cell line could affect the responsiveness to metformin *in vitro*. In the six cell lines analyzed in this study, the expression of LKB1 was perfectly correlated with the reactivity to metformin; however, this observation does not rule out that low OCT1 expression abolishes the reactivity to metformin *in vitro*.

AICAR-induced AMPK activation was observed in previous studies using isolated hepatocytes from mice (Foretz et al., 2010) and rats (Corton et al., 1995) and, in the present study, using hepatic cancer-derived HepG2 cells (Figure 2B). However, only a few reports described similar results *in vivo*. After two weeks of administration of AICAR, AMPK activity in the liver is increased approximately two-fold in mice (Liu et al., 2015). To our knowledge, only two studies reported *in vivo* AMPK activation after acute administration of AICAR (Buhl et al., 2002; Sajan et al., 2010). By using obese Zucker (*fa/fa*) rats and Sprague-Dawley rats, the authors reported a two- to three-fold increase of AMPK activity and pAMPK (Thr¹⁷²) by AICAR and a three-fold increase by metformin, indicating that metformin more potentially activates AMPK in the liver than does AICAR. We also found AMPK activation by metformin in the liver but failed to detect the effect of AICAR (Figure 4). The discrepancy may be ascribable to the difference between mice and rats. Because AICAR must be transported into the liver and phosphorylated to yield ZMP for its action, the kinetics of AMPK activation by AICAR may be influenced by the transporters and kinases, of which activity may vary among species and organs. Although the mechanism of muscle-specific action of AICAR in mice is elusive, these findings give us a clue to understanding the effectiveness of metformin for type 2 diabetes mellitus and AICAR for sports doping, respectively (Hardie et al., 2012). Because many pro-AMPK reagents exert their effect through decreasing intracellular ATP concentration, use of transgenic mice expressing FRET biosensors for ATP (Imamura et al., 2009) will also be informative in understanding the regulation of AMPK *in vivo*.

In summary, we generated a highly sensitive AMPK biosensor, AMPKAR-EV, and established a protocol to visualize AMPK

activity in living mice. These transgenic mice expressing AMPKAR-EV will be a powerful tool for understanding AMPK activity in individual cell types and organs. Because the importance of the AMPK pathway has been identified in autophagy, aging, immunity, and inflammation, in addition to cancer and metabolism, AMPKAR-EV mice are expected to provide valuable information about AMPK activity in various fields.

EXPERIMENTAL PROCEDURES

For detailed methods, see also [Supplemental Experimental Procedures](#).

AMPKAR-EV Mice

The animal protocols were reviewed and approved by the Animal Care and Use Committee of Kyoto University Graduate School of Medicine (No. 14079, 15064, 16038, and 17539). To develop transgenic mice expressing AMPKAR-EV, Lox-Stop-Lox (LSL)-tdKeima-AMPKAR-EV mice were generated by cytoplasmic microinjection into fertilized eggs of B6C3F1 mice with Tol2 mRNA and pT2A-derived LSL-tdKeima-AMPKAR-EV vector as described previously (Sumiyama et al., 2010). Transgenic male mice were crossed with B6.FVB-Tg (Ella-cre)^{C5379Lmgd/J} female mice (a gift from Mitinori Saitou, Kyoto University, Kyoto, Japan) for the ubiquitous expression of AMPKAR-EV. Mice were backcrossed with C57BL/6 for at least two generations before analyses. Mice were housed in a specific pathogen-free facility and received a routine chow diet and water *ad libitum*. To date, no disease or anomaly has been associated with the transgenic mice used in this study. 4- to 40-week-old male and female mice were used for the *in vivo* imaging.

Plasmids

The AMPKAR-EV was generated by substitution of the kinase substrate peptide in the previously described Eevee backbone (Komatsu et al., 2011). From the N terminus, AMPKAR-EV consists of YPet, a spacer (Leu-Glu), the FHA1 domain of yeast Rad53 (aa 241–382), a spacer (Gly-Thr), the EV linker, a spacer (Ser-Gly), the substrate peptide (GSGEGSTKMRRVATLVLDGTGG SEL), a spacer (Gly-Gly-Arg), SECFP, a spacer (Ser-Arg), and the nuclear export signal peptide of the HIV-1 Rev protein (LQLPPLERLTL).

The cDNA of AMPKAR-EV was inserted into pPBsrs, consisting of a piggyBac transposon vector (Yusa et al., 2009). pCMV-mPBBase (mammalian codon-optimized PBBase) encoding a piggyBac transposase was a gift from Allan Bradley (Wellcome Trust Sanger Institute, Cambridge, UK).

Observation of the Skeletal Muscle and the Liver

Living mice were observed with an FV1000MVE inverted microscope (Olympus, Tokyo, Japan) equipped with a UplanSApo 30×/1.05 silicon oil-immersion objective lens (Olympus) or an FV1200MPE-BX61WI upright microscope (Olympus) equipped with a UplanSApo 25×/1.05 numerical aperture (NA) water-immersion objective lens (Olympus). The microscopes were equipped with an InSight DeepSee Ultrafast laser (0.95 W at 900 nm) (Spectra Physics, Mountain View, CA). The scan speed was set for 2 to 12.5 μs/pixel. The excitation wavelength for CFP was 840 nm, and that for NAD(P)H was 780 nm. Fluorescent images were acquired with the following filters and mirrors: an infrared (IR)-cut filter, BA685RIF-3; two dichroic mirrors, DM505 and DM570; and three emission filters, FF01-425/30 (Semrock, Rochester, NY) for second harmonic generation (SHG) and NAD(P)H, BA460-500 (Olympus) for CFP, and BA520-560 (Olympus) for FRET. The microscopes were equipped with a two-channel GaAsP detector unit and two multialkali detectors. FluoView software (Olympus) was used to control the microscope and to acquire images, which were saved in the multilayer 12-bit tagged image file format. Acquired images were processed and analyzed with Metamorph software as described previously (Kamioka et al., 2012). Intravital mouse imaging was performed essentially as described previously (Kamioka et al., 2012). For observation of the skeletal muscle, the mouse was placed in the prone position on an electric heat pad maintained at 37°C. The skin over the thigh was flapped to expose approximately 1 cm² of the biceps femoris, which was set over the objective. For observation of the liver, the abdominal wall

was incised to expose approximately 0.25 cm² of the tissue. The exposed tissue was imaged using an aspiration fixation system (Sano et al., 2016). Drugs were injected intravenously during imaging.

Energy Stress Manipulation

For electrically induced muscle contraction, the femoral nerve was stimulated with a NEPA21 electroporator (Nepa Gene, Chiba, Japan) at a voltage of 40 V. A tetanic contraction was obtained using 180 pulses at 5 Hz (O'Neill et al., 2011; Pratt and Lovering, 2014). Immediately after the stimulation, mice were anesthetized and subjected to *in vivo* imaging, which started approximately 5 min and no later than 31 min after the end of stimulation; in no case were images captured later than 40 min after the stimulation.

For the detection of exercise-induced AMPK activation, according to a previous report (Maarbjerg et al., 2009), mice were acclimatized to treadmill running before the experiment from day –5 to day –2 using an MK-680 treadmill (Muromachi-Koki, Tokyo, Japan). Initially, mice were allowed to rest in the treadmill apparatus for 10 min and then exercised by running for 5 min at 10 m/min and 5 min at 16 m/min at 0% incline. Before imaging, mice ran for 60 min at 16 m/min on a 0% incline. If necessary, electrical shock was applied to encourage running during both the acclimatization and the experiment. Immediately after the exercising, mice were anesthetized and subjected to *in vivo* imaging, which started 6 to 25 min after the end of exercising; in no case were images captured later than 40 min after the exercising (Figure S3).

For fasting, mice were single-caged and maintained in standard cages without accesses to food for more than 24 or 48 hr. To confirm fasting status, blood glucose levels were measured using a blood glucose monitor (Glutest Neo Sensor; Sanwa Kagaku Kenkyusho, Nagoya, Japan). Histochemical analysis of NADH tetrazolium reductase (NADH-TR) was performed as previously described (Hoshino et al., 2013).

Quantification and Statistical Analysis

The statistical differences between the two experimental groups were assessed by Student's two-sample t test.

SUPPLEMENTAL INFORMATION

Supplemental Information includes Supplemental Experimental Procedures, three figures, and one movie and can be found with this article online at <https://doi.org/10.1016/j.celrep.2017.10.113>.

AUTHOR CONTRIBUTIONS

Y. Konagaya performed most of the experiments. Y.H. performed part of the experiments. K. Takakura, M.I., and Y. Kamioka supported the experiments. N.S., A.K., K.S., and T.A. provided resources. Y. Konagaya, K. Terai, and M.M. analyzed results, designed the project, and wrote the manuscript.

ACKNOWLEDGMENTS

We are grateful to the members of the Matsuda laboratory for their helpful input; Y. Inaoka, K. Hirano, S. Kobayashi, N. Koizumi, and A. Kawagishi for their technical assistance; and the Medical Research Support Center of Kyoto University for *in vivo* imaging. K. Terai was funded by JSPS KAKENHI 16K19391. M.M. was funded by JSPS KAKENHI 15H02397, 15H05949 "Resonance Bio," and 16H06280 "ABIS"; CREST JPMJCR1654; and the Nakatani Foundation.

Received: April 4, 2017

Revised: September 28, 2017

Accepted: October 27, 2017

Published: November 28, 2017

REFERENCES

Buhl, E.S., Jessen, N., Pold, R., Ledet, T., Flyvbjerg, A., Pedersen, S.B., Pedersen, O., Schmitz, O., and Lund, S. (2002). Long-term AICAR administration

reduces metabolic disturbances and lowers blood pressure in rats displaying features of the insulin resistance syndrome. *Diabetes* 51, 2199–2206.

Carling, D., Thornton, C., Woods, A., and Sanders, M.J. (2012). AMP-activated protein kinase: new regulation, new roles? *Biochem. J.* 445, 11–27.

Chen, Y., Zhou, K., Wang, R., Liu, Y., Kwak, Y.-D., Ma, T., Thompson, R.C., Zhao, Y., Smith, L., Gasparini, L., et al. (2009). Antidiabetic drug metformin (GlucophageR) increases biogenesis of Alzheimer's amyloid peptides via up-regulating BACE1 transcription. *Proc. Natl. Acad. Sci. USA* 106, 3907–3912.

Cho, K., Chung, J.Y., Cho, S.K., Shin, H.-W., Jang, I.-J., Park, J.-W., Yu, K.-S., and Cho, J.-Y. (2015). Antihyperglycemic mechanism of metformin occurs via the AMPK/LXR α /POMC pathway. *Sci. Rep.* 5, 8145.

Cool, B., Zinker, B., Chiou, W., Kifle, L., Cao, N., Perham, M., Dickinson, R., Adler, A., Gagne, G., Iyengar, R., et al. (2006). Identification and characterization of a small molecule AMPK activator that treats key components of type 2 diabetes and the metabolic syndrome. *Cell Metab.* 3, 403–416.

Corton, J.M., Gillespie, J.G., Hawley, S.A., and Hardie, D.G. (1995). 5-aminoimidazole-4-carboxamide ribonucleoside. a specific method for activating AMP-activated protein kinase in intact cells? *Eur. J. Biochem.* 229, 558–565.

Davies, S.P., Helps, N.R., Cohen, P.T.W., and Hardie, D.G. (1995). 5'-AMP inhibits dephosphorylation, as well as promoting phosphorylation, of the AMP-activated protein kinase. Studies using bacterially expressed human protein phosphatase-2C α and native bovine protein phosphatase-2AC. *FEBS Lett.* 377, 421–425.

Duan, Y., Zhang, R., Zhang, M., Sun, L., Dong, S., Wang, G., Zhang, J., and Zhao, Z. (2013). Metformin inhibits food intake and neuropeptide Y gene expression in the hypothalamus. *Neural Regen. Res.* 8, 2379–2388.

Dzamko, N., Schertzer, J.D., Ryall, J.G., Steel, R., Macaulay, S.L., Wee, S., Chen, Z.-P., Michell, B.J., Oakhill, J.S., Watt, M.J., et al. (2008). AMPK-independent pathways regulate skeletal muscle fatty acid oxidation. *J. Physiol.* 586, 5819–5831.

Foretz, M., Hébrard, S., Leclerc, J., Zarrinpashneh, E., Soty, M., Mithieux, G., Sakamoto, K., Andreelli, F., and Viollet, B. (2010). Metformin inhibits hepatic gluconeogenesis in mice independently of the LKB1/AMPK pathway via a decrease in hepatic energy state. *J. Clin. Invest.* 120, 2355–2369.

Göransson, O., McBride, A., Hawley, S.A., Ross, F.A., Shpiro, N., Foretz, M., Viollet, B., Hardie, D.G., and Sakamoto, K. (2007). Mechanism of action of A-769662, a valuable tool for activation of AMP-activated protein kinase. *J. Biol. Chem.* 282, 32549–32560.

Gowans, G.J., Hawley, S.A., Ross, F.A., and Hardie, D.G. (2013). AMP is a true physiological regulator of AMP-activated protein kinase by both allosteric activation and enhancing net phosphorylation. *Cell Metab.* 18, 556–566.

Hardie, D.G., Ross, F.A., and Hawley, S.A. (2012). AMPK: a nutrient and energy sensor that maintains energy homeostasis. *Nat. Rev. Mol. Cell Biol.* 13, 251–262.

Hawley, S.A., Boudeau, J., Reid, J.L., Mustard, K.J., Udd, L., Mäkelä, T.P., Alessi, D.R., and Hardie, D.G. (2003). Complexes between the LKB1 tumor suppressor, STRAD α /beta and MO25 α /beta are upstream kinases in the AMP-activated protein kinase cascade. *J. Biol.* 2, 28.

Hawley, S.A., Pan, D.A., Mustard, K.J., Ross, L., Bain, J., Edelman, A.M., Frenquelli, B.G., and Hardie, D.G. (2005). Calmodulin-dependent protein kinase kinase- β is an alternative upstream kinase for AMP-activated protein kinase. *Cell Metab.* 2, 9–19.

Hinke, S.A., Martens, G.A., Cai, Y., Finsi, J., Heimberg, H., Pipeleers, D., and Van de Castele, M. (2007). Methyl succinate antagonises biguanide-induced AMPK-activation and death of pancreatic beta-cells through restoration of mitochondrial electron transfer. *Br. J. Pharmacol.* 150, 1031–1043.

Hoshino, S., Sakamoto, K., Vassilopoulos, S., Camus, S.M., Griffin, C.A., Esk, C., Torres, J.A., Ohkoshi, N., Ishii, A., Tamaoka, A., et al. (2013). The CHC22 clathrin-GLUT4 transport pathway contributes to skeletal muscle regeneration. *PLoS ONE* 8, e77787.

Hurley, R.L., Anderson, K.A., Franzone, J.M., Kemp, B.E., Means, A.R., and Witters, L.A. (2005). The Ca²⁺/calmodulin-dependent protein kinase kinases are AMP-activated protein kinase kinases. *J. Biol. Chem.* 280, 29060–29066.

- Imamura, H., Nhat, K.P., Togawa, H., Saito, K., Iino, R., Kato-Yamada, Y., Nagai, T., and Noji, H. (2009). Visualization of ATP levels inside single living cells with fluorescence resonance energy transfer-based genetically encoded indicators. *Proc. Natl. Acad. Sci. USA* *106*, 15651–15656.
- Jensen, T.E., Rose, A.J., Jørgensen, S.B., Brandt, N., Schjerling, P., Wojtaszewski, J.F.P., and Richter, E.A. (2007). Possible CaMKK-dependent regulation of AMPK phosphorylation and glucose uptake at the onset of mild tetanic skeletal muscle contraction. *Am. J. Physiol. Endocrinol. Metab.* *292*, E1308–E1317.
- Jørgensen, S.B., Viollet, B., Andreelli, F., Frøsig, C., Birk, J.B., Schjerling, P., Vaulont, S., Richter, E.A., and Wojtaszewski, J.F.P. (2004). Knockout of the $\alpha 2$ but not $\alpha 1$ 5'-AMP-activated protein kinase isoform abolishes 5-aminoimidazole-4-carboxamide-1- β -D-ribofuranoside but not contraction-induced glucose uptake in skeletal muscle. *J. Biol. Chem.* *279*, 1070–1079.
- Kamioka, Y., Sumiyama, K., Mizuno, R., Sakai, Y., Hirata, E., Kiyokawa, E., and Matsuda, M. (2012). Live imaging of protein kinase activities in transgenic mice expressing FRET biosensors. *Cell Struct. Funct.* *37*, 65–73.
- Khanal, P., Kim, G., Yun, H.J., Cho, H.G., and Choi, H.S. (2013). The prolyl isomerase Pin1 interacts with and downregulates the activity of AMPK leading to induction of tumorigenicity of hepatocarcinoma cells. *Mol. Carcinog.* *52*, 813–823.
- Kim, I., and He, Y.Y. (2013). Targeting the AMP-activated protein kinase for cancer prevention and therapy. *Front. Oncol.* *3*, 175.
- Kisfalvi, K., Eibl, G., Sinnett-Smith, J., and Rozengurt, E. (2009). Metformin disrupts crosstalk between G protein-coupled receptor and insulin receptor signaling systems and inhibits pancreatic cancer growth. *Cancer Res.* *69*, 6539–6545.
- Komatsu, N., Aoki, K., Yamada, M., Yukinaga, H., Fujita, Y., Kamioka, Y., and Matsuda, M. (2011). Development of an optimized backbone of FRET biosensors for kinases and GTPases. *Mol. Biol. Cell* *22*, 4647–4656.
- Kristensen, J.M., Treebak, J.T., Schjerling, P., Goodyear, L., and Wojtaszewski, J.F.P. (2014). Two weeks of metformin treatment induces AMPK-dependent enhancement of insulin-stimulated glucose uptake in mouse soleus muscle. *Am. J. Physiol. Endocrinol. Metab.* *306*, E1099–E1109.
- Liu, S., Jing, F., Yu, C., Gao, L., Qin, Y., and Zhao, J. (2015). AICAR-induced activation of AMPK inhibits TSH/SREBP-2/HMGCR pathway in liver. *PLoS ONE* *10*, e0124951.
- Maarbjerg, S.J., Jørgensen, S.B., Rose, A.J., Jeppesen, J., Jensen, T.E., Treebak, J.T., Birk, J.B., Schjerling, P., Wojtaszewski, J.F.P., and Richter, E.A. (2009). Genetic impairment of AMPK $\alpha 2$ signaling does not reduce muscle glucose uptake during treadmill exercise in mice. *Am. J. Physiol. Endocrinol. Metab.* *297*, E924–E934.
- Mihaylova, M.M., and Shaw, R.J. (2011). The AMPK signalling pathway coordinates cell growth, autophagy and metabolism. *Nat. Cell Biol.* *13*, 1016–1023.
- Nakatsu, Y., Iwashita, M., Sakoda, H., Ono, H., Nagata, K., Matsunaga, Y., Fukushima, T., Fujishiro, M., Kushiya, A., Kamata, H., et al. (2015). Prolyl isomerase Pin1 negatively regulates AMP-activated protein kinase (AMPK) by associating with the CBS domain in the γ subunit. *J. Biol. Chem.* *290*, 24255–24266.
- Narkar, V.A., Fan, W., Downes, M., Yu, R.T., Jonker, J.W., Alaynick, W.A., Banayo, E., Karunasiri, M.S., Lorca, S., and Evans, R.M. (2011). Exercise and PGC-1 α -independent synchronization of type I muscle metabolism and vasculature by ERR γ . *Cell Metab.* *13*, 283–293.
- Nguyen, A.W., and Daugherty, P.S. (2005). Evolutionary optimization of fluorescent proteins for intracellular FRET. *Nat. Biotechnol.* *23*, 355–360.
- O'Neill, H.M., Maarbjerg, S.J., Crane, J.D., Jeppesen, J., Jørgensen, S.B., Schertzer, J.D., Shyroka, O., Kiens, B., van Denderen, B.J., Tarnopolsky, M.A., et al. (2011). AMP-activated protein kinase (AMPK) $\beta 1\beta 2$ muscle null mice reveal an essential role for AMPK in maintaining mitochondrial content and glucose uptake during exercise. *Proc. Natl. Acad. Sci. USA* *108*, 16092–16097.
- Piston, D.W., Masters, B.R., and Webb, W.W. (1995). Three-dimensionally resolved NAD(P)H cellular metabolic redox imaging of the in situ cornea with two-photon excitation laser scanning microscopy. *J. Microsc.* *178*, 20–27.
- Pratt, S.J.P., and Lovering, R.M. (2014). A stepwise procedure to test contractility and susceptibility to injury for the rodent quadriceps muscle. *J. Biol. Methods* *1*, e8.
- Rothstein, E.C., Carroll, S., Combs, C.A., Jobsis, P.D., and Balaban, R.S. (2005). Skeletal muscle NAD(P)H two-photon fluorescence microscopy in vivo: topology and optical inner filters. *Biophys. J.* *88*, 2165–2176.
- Sajan, M.P., Bandyopadhyay, G., Miura, A., Standaert, M.L., Nimal, S., Longnus, S.L., Van Obberghen, E., Hainault, I., Fougelle, F., Kahn, R., et al. (2010). AICAR and metformin, but not exercise, increase muscle glucose transport through AMPK-, ERK-, and PDK1-dependent activation of atypical PKC. *Am. J. Physiol. Endocrinol. Metab.* *298*, E179–E192.
- Sample, V., Ramamurthy, S., Gorshkov, K., Ronnett, G.V., and Zhang, J. (2015). Polarized activities of AMPK and BRSK in primary hippocampal neurons. *Mol. Biol. Cell* *26*, 1935–1946.
- Sano, T., Kobayashi, T., Negoro, H., Sengiku, A., Hiratsuka, T., Kamioka, Y., Liou, L.S., Ogawa, O., and Matsuda, M. (2016). Intravital imaging of mouse urothelium reveals activation of extracellular signal-regulated kinase by stretch-induced intravesical release of ATP. *Physiol. Rep.* *4*, e13033.
- Shackelford, D.B., Abt, E., Gerken, L., Vasquez, D.S., Seki, A., Leblanc, M., Wei, L., Fishbein, M.C., Czernin, J., Mischel, P.S., and Shaw, R.J. (2013). LKB1 inactivation dictates therapeutic response of non-small cell lung cancer to the metabolism drug phenformin. *Cancer Cell* *23*, 143–158.
- Shaw, R.J., Kosmatka, M., Bardeesy, N., Hurley, R.L., Witters, L.A., DePinho, R.A., and Cantley, L.C. (2004). The tumor suppressor LKB1 kinase directly activates AMP-activated kinase and regulates apoptosis in response to energy stress. *Proc. Natl. Acad. Sci. USA* *101*, 3329–3335.
- Shaw, R.J., Lamia, K.A., Vasquez, D.S., Koo, S.H., Bardeesy, N., Depinho, R.A., Montminy, M., and Cantley, L.C. (2005). The kinase LKB1 mediates glucose homeostasis in liver and therapeutic effects of metformin. *Science* *310*, 1642–1646.
- Sinnett-Smith, J., Kisfalvi, K., Kui, R., and Rozengurt, E. (2013). Metformin inhibition of mTORC1 activation, DNA synthesis and proliferation in pancreatic cancer cells: dependence on glucose concentration and role of AMPK. *Biochem. Biophys. Res. Commun.* *430*, 352–357.
- Sumiyama, K., Kawakami, K., and Yagita, K. (2010). A simple and highly efficient transgenesis method in mice with the Tol2 transposon system and cytoplasmic microinjection. *Genomics* *95*, 306–311.
- Suter, M., Riek, U., Tuerk, R., Schlattner, U., Wallimann, T., and Neumann, D. (2006). Dissecting the role of 5'-AMP for allosteric stimulation, activation, and deactivation of AMP-activated protein kinase. *J. Biol. Chem.* *281*, 32207–32216.
- Tajima, K., Nakamura, A., Shirakawa, J., Togashi, Y., Orime, K., Sato, K., Inoue, H., Kaji, M., Sakamoto, E., Ito, Y., et al. (2013). Metformin prevents liver tumorigenesis induced by high-fat diet in C57Bl/6 mice. *Am. J. Physiol. Endocrinol. Metab.* *305*, E987–E998.
- Tsou, P., Zheng, B., Hsu, C.H., Sasaki, A.T., and Cantley, L.C. (2011). A fluorescent reporter of AMPK activity and cellular energy stress. *Cell Metab.* *13*, 476–486.
- Viollet, B., Guigas, B., Sanz Garcia, N., Leclerc, J., Foretz, M., and Andreelli, F. (2012). Cellular and molecular mechanisms of metformin: an overview. *Clin. Sci.* *122*, 253–270.
- Wang, D.S., Jonker, J.W., Kato, Y., Kusuhabara, H., Schinkel, A.H., and Sugiyama, Y. (2002). Involvement of organic cation transporter 1 in hepatic and intestinal distribution of metformin. *J. Pharmacol. Exp. Ther.* *302*, 510–515.
- Woods, A., Johnstone, S.R., Dickerson, K., Leiper, F.C., Fryer, L.G.D., Neumann, D., Schlattner, U., Wallimann, T., Carlson, M., and Carling, D. (2003). LKB1 is the upstream kinase in the AMP-activated protein kinase cascade. *Curr. Biol.* *13*, 2004–2008.
- Xiao, B., Sanders, M.J., Carmena, D., Bright, N.J., Haire, L.F., Underwood, E., Patel, B.R., Heath, R.B., Walker, P.A., Hallen, S., et al. (2013). Structural

basis of AMPK regulation by small molecule activators. *Nat. Commun.* **4**, 3017.

Yusa, K., Rad, R., Takeda, J., and Bradley, A. (2009). Generation of transgene-free induced pluripotent mouse stem cells by the piggyBac transposon. *Nat. Methods* **6**, 363–369.

Zhang, B.B., Zhou, G., and Li, C. (2009). AMPK: an emerging drug target for diabetes and the metabolic syndrome. *Cell Metab.* **9**, 407–416.

Zhang, Y.L., Guo, H., Zhang, C.S., Lin, S.Y., Yin, Z., Peng, Y., Luo, H., Shi, Y., Lian, G., Zhang, C., et al. (2013). AMP as a low-energy charge signal autonomously initiates assembly of AXIN-AMPK-LKB1 complex for AMPK activation. *Cell Metab.* **18**, 546–555.

Zhou, X.Z., and Lu, K.P. (2016). The isomerase PIN1 controls numerous cancer-driving pathways and is a unique drug target. *Nat. Rev. Cancer* **16**, 463–478.